A Comparison of Higher Order Boussinesq and Local Polynomial Approximation Models

Maurício F. Gobbi[1], Andrew B. Kennedy[2] and James T. Kirby[2]

Abstract

Two recent approaches for computing wave evolution over varying topography are presented: the high order Boussinesq model of Gobbi and Kirby (1998) and the local polynomial approximation (LPA) method of Kennedy and Fenton (1997). Both analytical results and numerical solutions of Gobbi and Kirby (1998) model and two variants of the LPA method are presented and compared with exact solutions and laboratory measurements of waves propagating over submerged features.

Introduction

The increasing availability of high-speed computers has encouraged several researchers to work towards implementing deterministic nonlinear models and their numerical solutions for more accurate predictions of wave transformation in coastal areas. A great deal of effort has been made to extend the validity of $O(\mu^2)$ ($\mu \sim$ depth to length ratio) Boussinesq-type models to both deeper water (eg. Nwogu, 1993; Schäffer *et al.*, 1995) and highly nonlinear conditions (Wei *et al.*, 1995). Recently, noticing that existing Boussinesq models, which assume a second degree polynomial approximation for the velocity potential's vertical (z) dependency, have poor kinematics prediction in deep water, Gobbi *et al.* (1998) have derived a new Boussinesq-type model for a flat bed, which assumes that the velocity potential has a fourth degree polynomial dependency in z. The model's dependent variables are defined to give a (4,4) Padé linear dispersion relationship, and is fully nonlinear. Comparisons of several linear and nonlinear properties with exact solutions show great improvement of Gobbi *et al.* (1998) over Wei *et al.* (1995). A variable depth version of the model has been derived by Gobbi and Kirby (1998), and comparisons with laboratory experimental data show, again, very significant improvement over the model by Wei *et al.* (1995). We shall refer to these fourth order models as GKW98.

---

[1]Simepar, Caixa Postal 360, Curitiba, PR 80001-970, Brazil.
[2]Center for Applied Coastal Research, University of Delaware, Newark, DE. 19716 USA.

Recently, several local polynomial approximation methods have been developed (Kennedy and Fenton, 1997) which seek to provide local solutions to Laplace's equation in a weighted residual sense by assuming a local polynomial for the velocity potential at each local subdomain, where a subdomain is bounded by the bottom, the free surface, and vertical interfaces. The solution is subject to bottom and free surface constraints and continuity of the velocity and velocity potential at the subdomains' interfaces. With the problem completely specified for a given time, the coefficients of the polynomial are calculated. The kinematic and dynamic free surface boundary conditions are then used to advance the solution in time, and provide new free surface constraints for the next time step. Of the several variants of LPA methods, in this paper we shall look at two cases: both with only one horizontal dimension and fully nonlinear, one with fourth degree (somewhat comparable to GKW98) and one with sixth degree polynomial vertical representation of the velocity potential.

We briefly present both the GKW98 and LPA models, and then look at analytical properties of the linearized models and Stokes second harmonic amplitudes. Finally, the models are compared with experimental data.

Fully Nonlinear, $O(\mu^4)$ Boussinesq Model

This model, which was derived by Gobbi and Kirby (1998), consists of a set of coupled evolution equations which approximate the mass flux and momentum conservation in an arbitrary depth located at elevation $z = -h(x, y)$, where (x, y) are the horizontal spatial coordinates. The dependent variables are the free surface displacement η and the weighted average of the eulerian velocity between two arbitrary elevations, z_a and z_b in the water column, $\tilde{u}$, with weight parameter β. The choice of of these elevations and the weight parameter are related to the accuracy of the linear dispersion properties of the model. The nondimensionalized mass conservation equation is given by

$$\eta_t + \nabla \cdot \mathbf{M} = 0; \quad \mathbf{M} = \int_{-h}^{\delta\eta} \nabla\phi dz, \tag{1}$$

with

$$
\begin{aligned}
\mathbf{M} &= H\left\{\tilde{u} + \mu^2\left[\left(Ah - \frac{H}{2}\right)(2\nabla h F_{22} + \nabla F_{21}) + \left(Bh^2 - \frac{H^2}{3}\right)\nabla F_{22}\right]\right.\\
&+ \mu^4\left[\left(Ah - \frac{H}{2}\right)(2\nabla h F_{42} + \nabla F_{41} + 2\nabla h F_{44} + \nabla F_{43})\right.\\
&+ \left(Bh^2 - \frac{H^2}{3}\right)(\nabla F_{42} + 3\nabla h F_{45} + \nabla F_{44})\\
&+ \left.\left.\left(Ch^3 - \frac{H^3}{4}\right)(4\nabla h F_{46} + \nabla F_{45}) + \left(Dh^4 - \frac{H^4}{5}\right)\nabla F_{46}\right]\right\},
\end{aligned} \tag{2}
$$

and $H = h + \delta\eta$. The pair of momentum conservation equations is given by

$$\mathbf{U}_t = -\nabla\eta - \frac{\delta}{2}\nabla\left(|\tilde{u}|^2\right) + \Gamma_1\left(\eta, \tilde{u}_t\right) + \Gamma_2\left(\eta, \tilde{u}\right), \tag{3}$$

where

$$\begin{aligned}
\mathbf{U} \equiv & \ \tilde{\mathbf{u}} + \mu^2 \left[(A-1) h \left(2\nabla h F_{22} + \nabla F_{21} \right) + (B-1) h^2 \nabla F_{22} \right] \\
+ & \ \mu^4 \left[(A-1) h \left(2\nabla h F_{42} + \nabla F_{41} + 2\nabla h F_{44} + \nabla F_{43} \right) \right. \\
+ & \ (B-1) h^2 \left(\nabla F_{42} + 3\nabla h F_{45} + \nabla F_{44} \right) \\
+ & \ \left. (C-1) h^3 \left(4\nabla h F_{46} + \nabla F_{45} \right) + (D-1) h^4 \nabla F_{46} \right]
\end{aligned} \tag{4}$$

$$\begin{aligned}
\Gamma_1 \equiv & \ \mu^2 \nabla \left[\delta \eta F_{21t} + \left(2h\delta\eta + \delta^2\eta^2 \right) F_{22t} \right] \\
+ & \ \mu^4 \nabla \left[\delta\eta \left(F_{41t} + F_{43t} \right) + \left(2h\delta\eta + \delta^2\eta^2 \right) \left(F_{42t} + F_{44t} \right) \right. \\
+ & \ \left(3h^2\delta\eta + 3h\delta^2\eta^2 + \delta^3\eta^3 \right) F_{45t} \\
+ & \ \left. \left(4h^3\delta\eta + 6h^2\delta^2\eta^2 + 4h\delta^3\eta^3 + \delta^4\eta^4 \right) F_{45t} \right]
\end{aligned} \tag{5}$$

$$\begin{aligned}
\Gamma_2 \equiv - & \ \mu^2 \delta \nabla \left\{ \tilde{\mathbf{u}} \cdot \left[(Ah - H) \left(\nabla F_{21} + 2\nabla h F_{22} \right) + \left(Bh^2 - H^2 \right) \nabla F_{22} \right] \right. \\
+ & \ \frac{1}{2} \left(F_{21} + 2H F_{22} \right)^2 \Big\} \\
- & \ \mu^4 \delta \nabla \left\{ \tilde{\mathbf{u}} \cdot \left[(Ah - H) \left(\nabla F_{41} + 2\nabla h F_{42} + \nabla F_{43} + 2\nabla h F_{44} \right) \right. \right. \\
+ & \ \left(Bh^2 - H^2 \right) \left(\nabla F_{42} + \nabla F_{44} + 3\nabla h F_{45} \right) \\
+ & \ \left. \left(Ch^3 - H^3 \right) \left(\nabla F_{45} + 4\nabla h F_{46} \right) + \left(Dh^4 - H^4 \right) \nabla F_{46} \right] \\
+ & \ \frac{1}{2} \left| (Ah - H) \left(\nabla F_{21} + 2\nabla h F_{22} \right) + \left(Bh^2 - H^2 \right) \nabla F_{42} \right|^2 \\
+ & \ \frac{1}{2} \left[\left(F_{21} + 2H F_{22} \right) \left(F_{41} + 2H F_{42} \right. \right. \\
+ & \ \left. \left. \left. F_{43} + 2H F_{44} + 3H^2 F_{45} + 4H^3 F_{46} \right) \right] \right\}
\end{aligned} \tag{6}$$

$$F_{21}(\tilde{\mathbf{u}}) \equiv G\nabla h \cdot \tilde{\mathbf{u}} \tag{7}$$

$$F_{22}(\tilde{\mathbf{u}}) \equiv \frac{1}{2} G\nabla \cdot \tilde{\mathbf{u}} \tag{8}$$

$$F_{41}(\tilde{\mathbf{u}}) \equiv -|\nabla h|^2 \left[(A-1)\nabla h \cdot \tilde{\mathbf{u}} + (B-A) h\nabla \cdot \tilde{\mathbf{u}} \right] \tag{9}$$

$$F_{42}(\tilde{\mathbf{u}}) \equiv -\frac{1}{2}\nabla^2 h \left[(A-1)\nabla h \cdot \tilde{\mathbf{u}} + (B-A) h\nabla \cdot \tilde{\mathbf{u}} \right] \tag{10}$$

$$F_{43}(\tilde{\mathbf{u}}) \equiv \nabla h \cdot \nabla \left(Ah\nabla h \cdot \tilde{\mathbf{u}} \right) + \frac{1}{2}\nabla h \cdot \nabla \left(Bh^2 \nabla \cdot \tilde{\mathbf{u}} \right) \tag{11}$$

$$\begin{aligned}
F_{44}(\tilde{\mathbf{u}}) \equiv & \ \frac{1}{2}\nabla^2 \left(Ah\nabla h \cdot \tilde{\mathbf{u}} \right) + \frac{1}{4}\nabla^2 \left(Bh^2 \nabla \cdot \tilde{\mathbf{u}} \right) \\
- & \ \frac{1}{2}\nabla^2 h\nabla h \cdot \tilde{\mathbf{u}} - \nabla h \cdot \nabla \left(\nabla h \cdot \tilde{\mathbf{u}} \right)
\end{aligned} \tag{12}$$

$$F_{45}(\tilde{\mathbf{u}}) \equiv -\frac{1}{6}\nabla^2 h\nabla \cdot \tilde{\mathbf{u}} - \frac{1}{3}\nabla h \cdot \nabla \left(\nabla \cdot \tilde{\mathbf{u}} \right) - \frac{1}{6}\nabla^2 \left(\nabla h \cdot \tilde{\mathbf{u}} \right) \tag{13}$$

$$F_{46}(\tilde{\mathbf{u}}) \equiv -\frac{1}{24}\nabla^2 \left(\nabla \cdot \tilde{\mathbf{u}} \right). \tag{14}$$

where $G \equiv \left(1 + \mu^2 |\nabla h|^2 \right)^{-1}$. The nondimensional parameters appearing are δ and μ, characterizing the importance of nonlinearity and dispersion, respectively.

For details on the derivation of the equations above, the values of A, B, C, D (functions of constants β, z_a/h, and z_b/h), and the numerical implementation, the reader is referred to Gobbi *et al.* (1998) and Gobbi and Kirby (1998).

Local Polynomial Approximation Method

The local polynomial approximation method is a finite depth, potential flow technique for computing wave evolution over varying topography. It was designed to provide high accuracy with a reasonable computational cost, and remains general enough that the order of approximation may be easily changed.

The local polynomial approximation method used here is identical to that presented in Kennedy and Fenton (1997). In contrast to the presentation there, where the numerical solution method was highlighted, it is presented here in as a dimensionless set of differential equations for the approximate solution of Laplace's equation coupled with potential flow evolution equations. The velocity potential ϕ is assumed to be represented in the vertical coordinate z, by a polynomial of arbitrary degree

$$\phi(x, z) = \sum_{j=0}^{n-1} A_j(x) z^j \tag{15}$$

where the A_j's are functions only of the horizontal coordinate. The level of approximation n controls the degree of polynomial used and hence the accuracy. Here, the levels of approximation $n = 5$ and $n = 7$ will be used which have, respectively, fourth and sixth degree polynomial approximations in the vertical direction z. The initially unknown functions A_j must be chosen to satisfy the bottom boundary condition at the bed location $z = -h(x)$

$$\phi_z + \phi_x h_x = 0 \ \text{ on } z = -h \tag{16}$$

and also the free surface boundary condition

$$\phi(x, z = \eta(x)) = \phi^{(s)}(x) \tag{17}$$

This leaves $n - 2$ constraints needed to completely specify the distribution of the A_j functions. These are found by imposing an approximation to the full field equation at collocation points in the vertical plane

$$\nabla^2 \phi = 0 \ \text{ on } z_j = -h + (\eta + h)\alpha_j, \ j = 1, 2, \ldots, n-2 \tag{18}$$

For all results presented here, collocation points, z_j, are taken to be the Gauss-Legendre points for $N = n - 2$, using the free surface and the bed as limits.

With the addition of global boundary conditions on the lateral boundaries, a set of block-banded linear equations results which completely specifies the problem. Once the system of equations has been solved, the flow field may be

determined and the free surface elevation and velocity potential may be advanced to the next time step using the free surface evolution equations

$$\eta_t = -\left(\int_{-h}^{\eta} \phi_x dz\right)_x \tag{19}$$

$$\phi_t^{(s)} = -\eta - \frac{1}{2}\left(\phi_x^2 + \phi_z^2\right) + \phi_z \eta_t \tag{20}$$

It is very simple to extend the system of equations to three dimensions, but because of computational considerations, this is not advisable. For one horizontal dimension, a good solution technique uses complex polynomials to represent the flow field as detailed in Kennedy and Fenton (1997), but this particular technique cannot be extended into an extra dimension.

Analytical Properties

For very small amplitude waves propagating over a level bottom, a progressive sinusoidal wave solution can be substituted into the linearized constant depth versions of both GKW98 and LPA to give an approximation to the exact linear dispersion relationship. Details can be found in Gobbi *et al.* (1998) for GKW98 dispersion, which results in a (4,4) Padé approximant to the exact relationship, and in Kennedy (1997) for the LPA formulations. Figure 1 shows the ratio to the exact solution of the linear phase speed calculated for GKW98, LPA $n = 5$, and LPA $n = 7$. It is clear that the GKW98 phase speed sits in between the two LPA results in terms of accuracy. Figures 2 and 3 show the vertical profile of the horizontal and vertical velocity amplitudes, respectively, normalized by their value at the free surface, for GKW98 and both LPA results. Notice the effect of the more powerful representation of the vertical dependence in LPA $n = 7$ over both GKW98 and LPA $n = 5$, which are quite comparable. Turning to a second order nonlinear property, figure 4 shows the ratio to the full theory solution of the amplitude of the second harmonic of a Stokes expansion of GKW98 and both LPA's. For this case, both LPA solutions give better result than the GKW98 model. This is probably because the GKW98 model was derived for optimized performance in a linear sense, whereas the LPA method uses the full water column in the specification of the problem.

Comparisons with Laboratory Measurements

In this section we compare the computations from GKW98 and both LPA implementations presented earlier with experimental data of waves propagating over submerged sills. First we use data from Beji and Battjes (1993) and Luth *et al.* (1994) consisting of regular waves propagating over a structure resembling a sand bar. Then we use the data from Ohyama *et al.* (1994) where the submerged structure has much steeper slopes, resembling a submerged breakwater. These two experiments have become quite popular for tests of wave propagation models, and the reader is referred to the original papers for additional information.
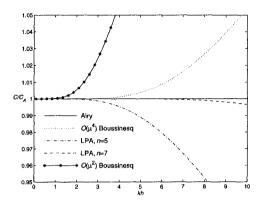
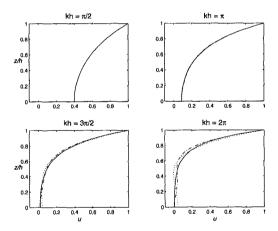Figure 1: Ratio to exact solution of phase speed.

Figure 2: Horizontal velocity profile. Exact (solid), GKW98 (dot), LPA n=5 (dash-dot), LPA n=7 (dash).
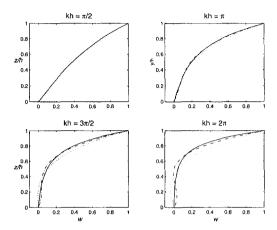
Figure 3: Vertical velocity profile. Exact (solid), GKW98 (dot), LPA n=5 (dash-dot), LPA n=7 (dash).
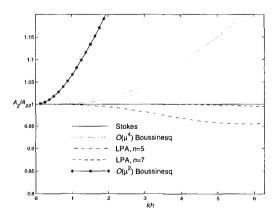

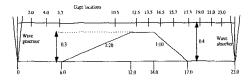Figure 4: Ratio to full problem solution of Stokes second harmonic amplitude.

Figure 5: Sketch of wave flume of Delft experiments. All dimensions in (m)

The experiments performed by Beji and Battjes (1993) and Luth *et al.* (1994) have the same geometric characteristics, except for the length scale in Luth *et al.* (1994), which is twice as large as in Beji and Battjes (1993). In Luth *et al.* (1994) all gauge locations used in Beji and Battjes (1993) were repeated, and another run of measurements was performed with the gauges at different locations. Here, we re-scale all measurements to the scales used in Beji and Battjes (1993). The layout of the experimental set-up with the locations of the measurement stations and the geometry of the flume are illustrated in Figure 5.

Three sets of data were collected using different incident wave conditions. We refer to these data sets as cases (a), (b), and (c). In case (b), wave breaking occurred and this case was disregarded. The incident wave amplitude and period were $0.01m$, $2.02s$, and $0.0205m$, $1.01s$, for cases (a) and (c) respectively.

In all cases, the data from gauges at $2.0m$ or $4.0m$ were used to synchronize the data with the models. Figures 6, 7, and 8 show, respectively, comparisons of GKW98, LPA $n = 7$, and LPA $n = 5$, with the case (a) of the Delft experimental data at several gauge locations. For this case, all three models' performance are quite satisfactory, with GKW98 and LPA $n = 7$ showing excellent agreement, while LPA $n = 5$ shows larger discrepancies, due to its less accurate linear phase speed. Similarly, figures 9, 10, and 11 show comparisons with case (c). Notice that because the incident waves in this case are shorter, it is a more demanding case than case (a), especially behind the bar, where nonlinear superharmonics are released as free waves, and are much shorter than the incident wave. For this case, LPA $n = 7$ performs best, followed by the also very good agreement of GKW98, but LPA $n = 5$ has poor agreement behind the structure. This result is in agreement with the linear phase speed results shown in figure 1.

We now compare the numerical results to the Ohyama experimental data. Summarizing the experimental setup, the wave flume is $65m$ long and $1.0m$ wide. The total depth of the flume is $1.6m$. The location of the center of the bar was $28.3m$ from the wavemaker. Figure 12 shows a sketch of the flume. Three tests with incident wave periods $1.34s$, $2.01s$, and $2.68s$, (cases 2, 4, 6, respectively) and fixed amplitude equal to $0.025m$ will be used in the comparisons. No wave breaking occurred in any of the tests. The time series were synchronized with the computations at station 3. Figures 12, 13, and 14 show the comparisons
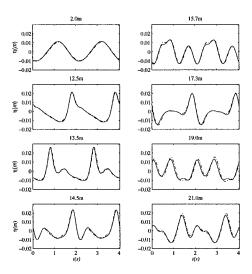
Figure 6: Comparisons of free surface displacement with case (a) of Delft experimental data at several gauge locations. GKW98 (dash-dot), data (solid).
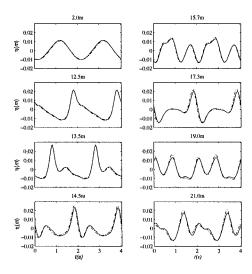

Figure 7: Comparisons of free surface displacement with case (a) of Delft experimental data at several gauge locations. LPA n=7 (dash-dot), data (solid).
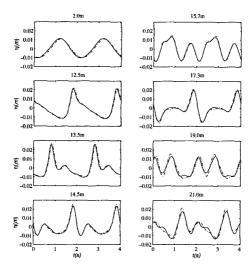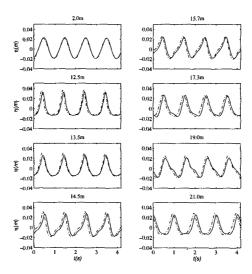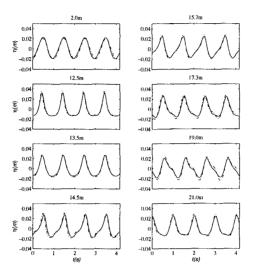
Figure 8: Comparisons of free surface displacement with case (a) of Delft exper-
imental data at several gauge locations. LPA n=5 (dash-dot), data (solid).

Figure 9: Comparisons of free surface displacement with case (c) of Delft exper-
imental data at several gauge locations. GKW98 (dash-dot), data (solid).

Figure 10: Comparisons of free surface displacement with case (c) of Delft experimental data at several gauge locations. LPA n=7 (dash-dot), data (solid).
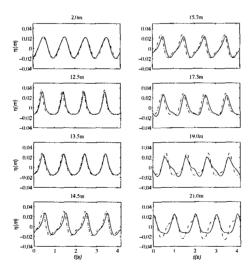

Figure 11: Comparisons of free surface displacement with case (c) of Delft experimental data at several gauge locations. LPA n=5 (dash-dot), data (solid).
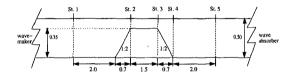
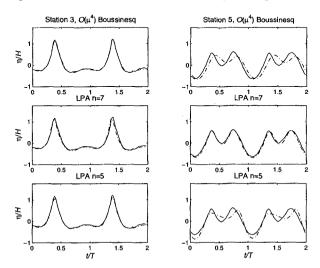Figure 12: Sketch of wave flume of the Ohyama experiment.

Figure 13: Comparisons of free surface displacement with case 2 of Ohyama experimental data. Computations (dash-dot), data (solid).

for the three cases, and it is possible to see that GKW98 and LPA $n = 5$ are comparable for cases 2 and 4, while LPA $n = 7$ outperforms them for these cases. In case 6, GKW98 and LPA $n = 7$ are comparable, while LPA $n = 5$ shows poorer performance. It might seem surprising that GKW98 does not perform in Ohyama cases 2 and 4 as well as in the Delft cases (a) and (c), since the incident wave conditions are not that different. This is due to the steep bottom slopes in Ohyama's cases which violates the intrinsic mild-slope assumption of GKW98 ($w \ll u$), which the fourth order polynomial for the potential's vertical dependence is not powerful enough to handle, for large enough μ.

Conclusions

Fully nonlinear local polynomial approximations and a $O(\mu^4)$ Boussinesq model were compared both in terms of analytical properties and of agreement
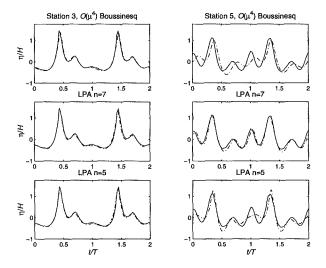
Figure 14: Comparisons of free surface displacement with case 4 of Ohyama experimental data. Computations (dash-dot), data (solid).
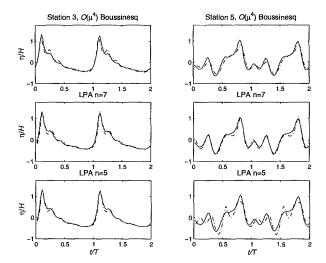

Figure 15: Comparisons of free surface displacement with case 6 of Ohyama experimental data. Computations (dash-dot), data (solid).

with experimental data. In general, because of its more accurate dispersion, the Boussinesq model performed better than the LPA with the same level of polynomial accuracy ($n = 5$), while the sixth degree polynomial LPA ($n = 7$) proved to be more accurate than both. The Boussinesq model has the advantage of being potentially faster in terms of computational time, and its 3-D implementation is more natural than the LPA methods shown here, which uses complex formulation to solve Laplace's equation and therefore cannot be extended to 3-D in an efficient manner. However, it is much simpler to extend the LPA model to any level of accuracy desired. The authors are now working on improvements in nonlinear behavior of Boussinesq models, improvements on dispersion properties of LPA methods, and 3-D implementation of the models.

Appendix: References

Beji, S. and Battjes, J. A., 1993 "Experimental investigations of wave propagation over a bar", *Coastal Eng.*, **19(1,2)**, 151-162.

Gobbi, M. F. and Kirby, J. T., 1998 "Wave evolution over submerged sills: tests of a high-order Boussinesq model", *Coastal Eng.*, Submitted.

Gobbi, M. F., Kirby, J. T., and Wei, G., 1998 "A fully nonlinear Boussinesq model for surface waves: II. Extension to $O(kh)^4$", *J. Fluid Mech.*, Submitted.

Kennedy, A. B., 1997, "The propagation of water waves over varying topography", Ph.D. Thesis, Monash University, Australia, 163pp..

Kennedy, A. B. and Fenton, J. D., 1997, "A fully-nonlinear computational method for wave propagation over topography", *Coastal Eng.*, **32**, 137-161.

Luth, H. R., Klopman, G., and Kitou, N., 1994 "Kinematics of a wave breaking partially on an offshore bar; LDV measurements with and without a net onshore current", Report H-1573. Delft Hydraulics, 40pp..

Nwogu, O., 1993 "An alternative form of Boussinesq equations for nearshore wave propagation", *J. Waterway, Port, Coast., Ocean Engng*, **119**, 618-638.

Ohyama, T., Kiota, W., and Tada, A., 1994 "Applicability of numerical models to nonlinear dispersive waves", *Coastal Eng.*, **24**, 297-213.

Schäffer, H. A. and Madsen, P. A., 1995 "Further enhencements of Boussinesq-type equations", *Coastal Eng.*, **26**, 1-14.

Wei, G., Kirby, J. T., Grilli, S. T., and Subramanya, R., 1995 " A fully nonlinear Boussinesq model for surface waves. Part 1. Highly nonlinear unsteady waves. *J. Fluid Mech.*, **294**, 71-92.